Trans Indian Inst Met
DOI 10.1007/s12666-016-0836-5

TECHNICAL PAPER

Microstructural Aspects of TIG and A-TIG Welding Process of Dissimilar Steel Grades and Correlation to Mechanical Behavior

Vishvesh J. Badheka[1] · Ritwik Basu[2] · Joseph Omale[3] · Jerzy Szpunar[3]

Received: 16 June 2015 / Accepted: 31 January 2016

Abstract The present study reports microstructural characteristics of two grades of steels, stainless steel (SS 304) and carbon steel welded using tungsten inert gas (TIG) and activated flux-TIG (A-TIG) processes. Activated fluxes such as TiO_2, ZnO and MnO_2 are effective for A-TIG welding of dissimilar weld between carbon steel to stainless steel. Mechanical properties, joint efficiency of A-TIG welds are found to be higher than normal TIG Welds. This study attempts to establish a correlation between observed mechanical behavior (hardness and strength) and the microstructural characteristics of the weld samples. Significant differences in microstructures are recorded in terms of grain size, local misorientation, grain and phase boundary characteristics in distinct regions of the welded samples. The microstructural observations exhibit: (1) the presence of Widmanstatten ferrite structure at the heat affected zone of the carbon steel part in the A-TIG welded specimen and (2) differences in structure at the interface of stainless steel and weld metal region under the two conditions of welding. These structures are morphologically different and shows differences in the number fraction of 45° <114> phase boundary orientation relationship. The microstructure also displays significant heterogeneity in grain size and grain misorientation.

✉ Vishvesh J. Badheka
vishvesh79@gmail.com; drvishvesh@gmail.com

[1] School of Technology, Pandit Deendayal Petroleum University, Raisan Village, Gandhinagar 382007, India

[2] Department of Mechanical Engineering, The Northcap University, Gurgaon 122017, India

[3] Department of Mechanical Engineering, University of Saskatchewan, 57 Campus Drive, Saskatoon S7N5A9, Canada

Keywords Tungsten inert gas (TIG) welding · Activated flux-TIG (A-TIG) welding · Electron backscattered diffraction (EBSD) · Local average misorientation · Orientation relationship · Grain boundary characteristics

1 Introduction

Gas tungsten arc welding (GTAW) more generically termed as tungsten inert gas (TIG) welding uses an arc between a non-consumable tungsten electrode and the work-pieces to be welded under a shielding gas. The technique has significance when it comes to welding of dissimilar metals and alloys. It is highly preferred in applications which require a high level of weld quality or considerable precision welding operation. However the drawbacks presented by this welding technique are the limited thickness of material which can be welded in a single pass, poor tolerance to some material composition and the low productivity. On the other hand, increase in the welding current leads to excessive widening of the weld width with no significant penetration [1–3]. This problem can be reduced by adopting activated tungsten inert gas (A-TIG) welding process that increases the penetration. A thin layer of flux is applied on the surface of the joint to be welded by brush before welding. The use of flux in A-TIG improves weld penetration for autogenous (without filler) welds [4]. In the present study ZnO has been used as a flux. The use of ZnO in A-TIG welds have been reported to increase the tensile strength and elongation to higher values when used in place of TiO_2 [1]. The strength of the A-TIG technique over conventional TIG practices is useful for joining dissimilar metals with thickness between 8 and 10 mm in a single pass. This allows full penetration of

Published online: 02 March 2016

welds, with no edge preparation. The penetration capability can be increased to 300 % when compared to conventional TIG welding process and the heat-to-heat variations in base metal compositions can be avoided when using the activated flux [4].This technique stands good where a transition in mechanical properties and high level of performance in service are desired. Typically austenitic stainless steel piping is most commonly used to contain high-temperature steam in power generation plants. However, below certain temperature and pressure, low-carbon and low-alloy steels can also perform adequately. Therefore transition from stainless steel to other form of steel is economic under certain conditions. Dissimilar metal joints find wide applications in chemical and power industries. For instance, super heater joints in boiler use 2.25Cr-1Mo steel tube joined with a particular grade of austenitic stainless steel. Most stainless steels can be successfully welded to low-carbon and low-alloy steels. However, consideration must be given to the effects of dilution of the weld metal with the two base metals and the different coefficients of thermal expansion in stainless steel and low-carbon or low-alloy steels which can affect the mechanical performance in the welded structures significantly [5]. The difficulties encountered in welding of dissimilar metals and alloys are the following:

(1) Differences in physical and mechanical properties of the two different materials that causes problems during welding and also in service.
(2) Choice of the filler material for compatibility with the base materials.
(3) Formation of intermetallic compounds at the interface which invariably embrittle the joints [6].

Details on experimental investigations including mechanical and metallurgical properties of TIG and ATIG welded joints are discussed vividly in few literature [1, 2]. Work is also being done in welding of P91 steel material through A-TIG process [7].

The mechanical strength in welded components is significantly altered by the distribution of non-homogenous strain that can arise due to mismatch in thermal coefficient at the weld bed, leading to local softening effect at the interface [8]. These strains can be quantified in terms of microstructural factors. Other factors which contribute to mechanical performance of these welds are grain size, grain boundary characteristics, distribution and size of precipitates, texture etc. Electron backscattered diffraction (EBSD) technique allows to measure the degree of strain in a localized region of a sample through change in the average in-grain misorientation which results from accumulation of dislocations. In addition, information on grains and grain boundaries, presence of phases, crystallographic orientation of grains can be gathered using this technique [9].

The early use of this technique have been restricted to characterization of deformed and annealed microstructures in metals and alloys processed through conventional deformation routes like rolling, forging, extrusion, sheet metal forming etc. [9]. However, no significant research applying this technique has been reported till date in the domain of welding technology. Available literatures report works on solid state welding especially friction stir welding and accumulative roll bonding [10–13].

Thus the objective of the present study is to perform a systematic microstructural investigation on dissimilar weld joints between stainless steel (SS) grade 304 and plain carbon steel (CS) using the two conditions of welding; tungsten inert gas (TIG) and A-TIG processes. This study attempts to explain the correlation between the observed mechanical behavior and microstructure. The regions of interest have been the heat affected zone (HAZ) and the fusion zone (FZ). Significant softening in the weld metal region occurs for the TIG welded specimen and that is reflected through low in-grain misorientation and increase in high angle boundaries (HAGBs) in the microstructure. Microstructure of the CS in the HAZ of the TIG welded specimen (N9) is not greatly altered from its parent counterpart; however the HAZ of the CS as represented in the A-TIG welded sample exhibit a structure resembling the Widmanstatten ferrite structure. The phase boundaries between SS and weld metal (WM) have been clearly different. Z8 (A-TIG welded under ZnO flux) exhibit an interlock structure of the two phases while N9 (TIG welded under double sided mode) exhibit a firm boundary interface. Further details on microstructural examination of the two welded specimens are presented in the following discussion.

2 Experimental Procedure

Chemical composition of the two grades of steel used for the study is presented in Table 1. TIG and A-TIG specimens used in this study were welded using Panasonic Make welding Machine (model BR1-200 (ac/dc)). Welding variables selected are included in Table 2. Both TIG and A-TIG welds were obtained under full penetration. The macrographs for both Z8 and N9 specimen are presented in Fig. 1; [1]. Prior to tensile test preparation, these welded specimens were machined on a vertical milling machine as per ASME section IX (QW-462.1d). Tensile tests were carried out in a SHIMADZU-AG-10NX to 10kNXplus tensile test unit. The dimensions of specimens are indicated in the schematic in Fig. 2a. During the tests, the strain rate was maintained at 2 mm/min. All tensile specimens

Table 1 Chemical compositions of SA516 Gr70 carbon steel and stainless steel (SS 304) materials

Materials	Alloying elements										
	C	Si	Mn	P	S	Cu	Ni	Cr	Mo	V	Al
CS	0.186	0.32	1.11	0.014	0.009	0.033	0.026	0.03	0.019	0.001	0.02
SS	0.064	0.250	1.020	0.025	0.006	–	8.20	18.45	0.021	–	–

Table 2 Welding Variables for GTA & A-TIG welds

Sample I.D	Flux	Current (Amp)	Travel speed (mm/min)	Arc voltage (volt)	Other welding variables
Experiment—1 root gap—1.5 mm					Electrode diameter: 3.0 mm
Z8	ZnO	200	55	13	Electrode tip angle: 60°
Experiment—2 root gap—1.0 mm					Arc gap: 2 mm
N9	Without flux	200	55	12.5	Shielding gas: Pure Argon (99.999)
					Gas flow rate: 12 lit/min
					Joint design: Open square
					2 % Thoriated tungsten electrode

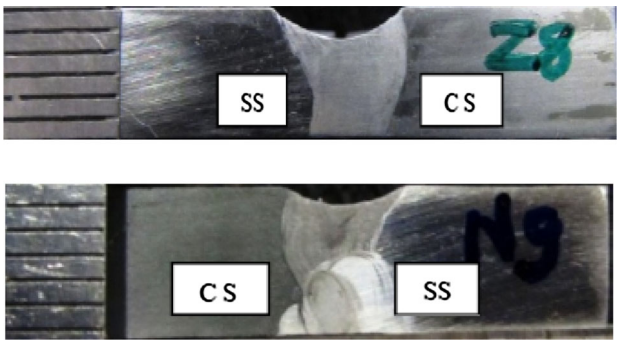

Fig. 1 Weld macrographs of Z8 and N9 specimens [1]

prepared from TIG and A-TIG processes failed on the CS side, as shown in Fig. 2b, c; [1]. Vickers hardness measurements were carried out across the weld section at 200 g load and a dwell time of 15 s. Indentations were typically performed at 3 mm spacing. For the electron back scattered diffraction (EBSD) measurements, samples were initially polished using conventional metallographic polishing techniques and finally colloidal silica polishing was used to generate a strain free surface. The measurements were carried out using a field emission scanning electron microscope (Hitachi SU 6600) coupled with an Oxford Instruments (OI) EBSD detector that acquired diffraction patterns using AZTEC 2.0 data acquisition software. The software indexes the diffraction patterns to evaluate the crystallographic orientation of the selected region. The microscope was operated with primary electron energy at 20 keV. Scans were performed at selected regions of the welded samples using a step size of 1.5 μm. The OI-HKL Channel 5 software was used to analyze the acquired EBSD data. This software allowed the identification of the grains and grain boundaries. Grain boundaries (GB) were defined as continuous regions of misorientation (misorientation angle >5°). GBs with a misorientation angle below 10° were considered as low angle GB (LAGB). Average misorientation was calculated within each grain at every measurement points with respect to all eight neighbour sites (in a square grid). Misorientations greater than 5° were neglected [8].

Residual stress (RS) measurements were conducted using a Bruker AXS general area detector system. Standard $\sin^2(\psi)$ method [14] was used for measurement of residual stress values at important diffraction peaks. The measurements were performed across the entire length of the welded samples at fixed distances. For residual stress, (002) peak was used. The residual stresses were calculated from the interplanar spacing for (hkl) pole through the following equation [14] as:

$$d_{hkl}(\psi\varphi) = d_0\left[1 + s_1(\sigma_{11} + \sigma_{22}) + \frac{1}{2}s_2\sigma_\varphi \sin^2\psi\right] \quad (1)$$

where ψ is the angle of inclination and φ is the rotation angle the goniometer has undergone at any instant of measurement. d_0 corresponds to the interplanar spacing of the unstrained material. s_1 and s_2 are the X-ray elastic constants, σ_{11} and σ_{22} are the stresses expressed in sample reference, and σ_φ is the residual stress of the material.

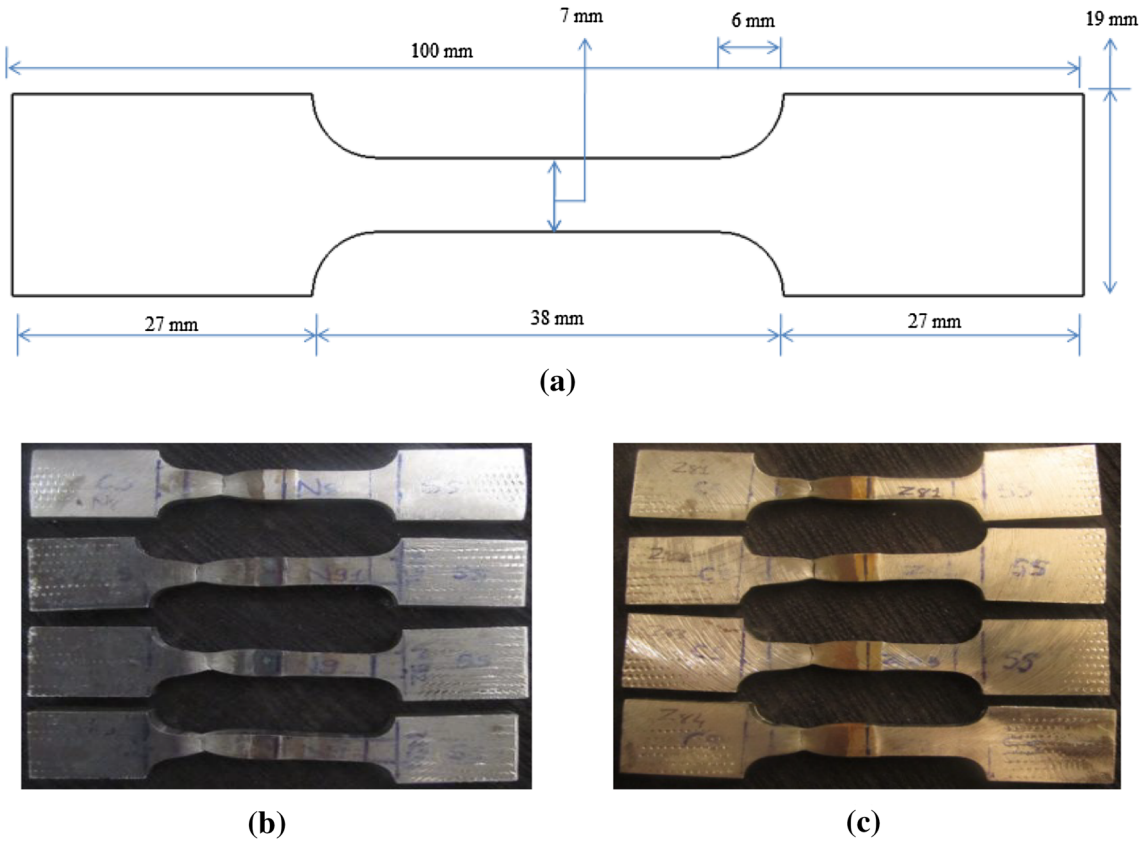

Fig. 2 **a** Dimensions of the tensile test specimen used in the present study. **b** N9 and **c** Z8 specimens. Both specimens failed on the CS side [1]

Table 3 Mechanical Properties of SA516 Gr70 Carbon Steel (CS), Stainless Steel (SS 304) and the Welded Specimens Z8 and N9

Main ID	Sub ID	Width (mm)	Thick (Mm)	Area (mm^2)	G.L. (mm)	F.L. (mm)	B.L load (KN)	TS (MPa)	Avg. TS (MPa)	% EL	Avg. % EL
Tensile test results for parent metals											
CS	CS1	7.5	6.40	48.02	39	47.95	26.21	547	**550**	22.9	**24**
	CS2	7.6	6.40	48.66	39	48.5	26.89	553		24.4	
SS	SS1	7.3	6.11	44.58	38	59.15	30.63	576	**624**	55.7	**56**
	SS2	7.3	6.10	44.57	38	59.35	29.93	672		56.2	
A TIG samples											
Z8	Z81	6.55	3.39	22.2	27	33.28	13.49	608	**609**	23.3	**25**
	Z82	7.8	3.64	28.42	30	37.6	16.85	593		25.3	
	Z83	7.8	3.83	29.89	31	38.7	18.58	609		24.8	
	Z84	8	4.32	34.57	33	41.2	21.61	625		24.8	
Normal TIG—single side and double side											
N9	N91	7.51	6.10	45.83	39	47.2	26.58	580	**584**	24.2	**25**
	N92	6.9	6.10	42.12	37	46.8	24.94	592		26.5	
	N93	6.5	6.13	39.85	36	44.5	23.07	579		23.6	

3 Results and Discussion

Table 3 presents the results on tensile test that has been performed on the two different welded specimens along with dimensions. No significant change in % elongation has been observed for the two specimens; A-TIG welded (Z8) and TIG welded (N9). However, Z8 shows higher tensile strength (TS) than N9. VHN micro hardness investigation reports higher average VHN values for N9 than Z8. As shown in the hardness-distance plot in Fig. 3, the difference in the peak values is distinct at the weld center. This difference is less significant towards HAZ on the SS side than on the CS side. It is also to be mentioned here that, though the estimated VHN of CS is more compared to SS in both Z8 and N9 weldments, it is seen that both the specimens fails on the CS side. This may be due to carbon migration from CS to SS that subsequently weakens the HAZ of the CS leading to failure. The joint efficiency of Normal-TIG in double side mode is 106 %. The efficiency increases to 110 % in A-TIG process.

Figures 4 and 5 presents the microstructure of the weld samples Z8 and N9 respectively. Both microstructures shows a clear difference between the HAZ and the base metal region on the SS side. The HAZ of SS shows presence of very large grains with orientations along the directions of the heat flow. No distinct differences exist between the HAZ and the base metal zone on the CS side. These differences in microstructures on the SS side arise due to sharp thermal gradients. This is because of lower thermal diffusivity of SS. The sharpness or steepness of thermal gradient is decided by the thermal diffusivity. Lower the thermal diffusivity, steeper is the thermal gradient. The thermal diffusivities reported for CS and SS are 11.72 and 4.2 mm^2/s respectively. However sample Z-8 shows much clear signature of grain coarsening than N9. The region of grain- coarsening and heat affected zone (HAZ) are critical in terms of embrittlement that are likely to concentrate in these areas. These morphologically oriented structure to some extent resemble certain solidification microstructure, where there is a directionality in grain growth depending on heat flow. Furthermore, it is reported that classical solidification theory can be applied to welding [15]. The CS in general shows an equiaxed ferritic microstructure. However, the heat-affected zone (HAZ) of CS in Z8 exhibits presence of Widmanstatten ferrite. Previous investigation reports shows that, HAZ undergoes a two phase transformation during cooling; a high temperature transformation of δ-Fe to γ-Fe followed by the γ-Fe to α-Fe in the second stage [16]. However the cooling rate also plays a very vital role in determining the weld microstructures. During welding, when all other material properties are uniform, the cooling rate will depend on the amount of molten metal and the availability of heat sink to conduct heat away from the melt. As in TIG welding, the weld pool is shallow and the energy of the arc causes a very high increase in temperature of the weld pool. Therefore the nuclei of austenite (γ) grains during δ-to-γ phase transformation grow by advancement of planar interface for a longer time in the HAZ while they are in the critical temperature. In the case of A-TIG welding, the weld pool is deeper and the volume of molten metal is larger. Therefore the arc energy does not heat up the weld pool to the same extent and the HAZ can cool down faster. Previous studies have shown that cooling rates are significantly increased during A-TIG welding of steels [17, 18]. Thus, the higher cooling rate in the A-TIG welding occurs by a massive transformation, leading to appearance of Widmanstatten structures.

More importantly, the combination of TIG and A-TIG welding intoduce differences in microstructural parametres

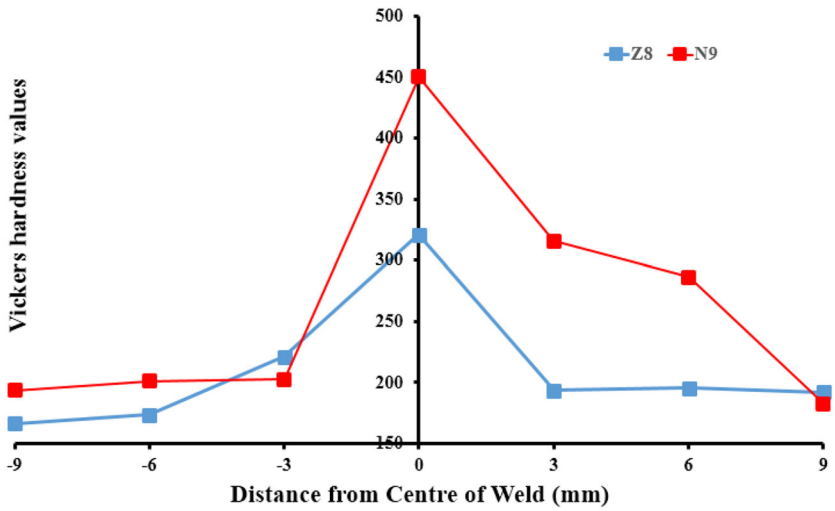

Fig. 3 Micro-hardness VHN as a function distance from the center of weld bead

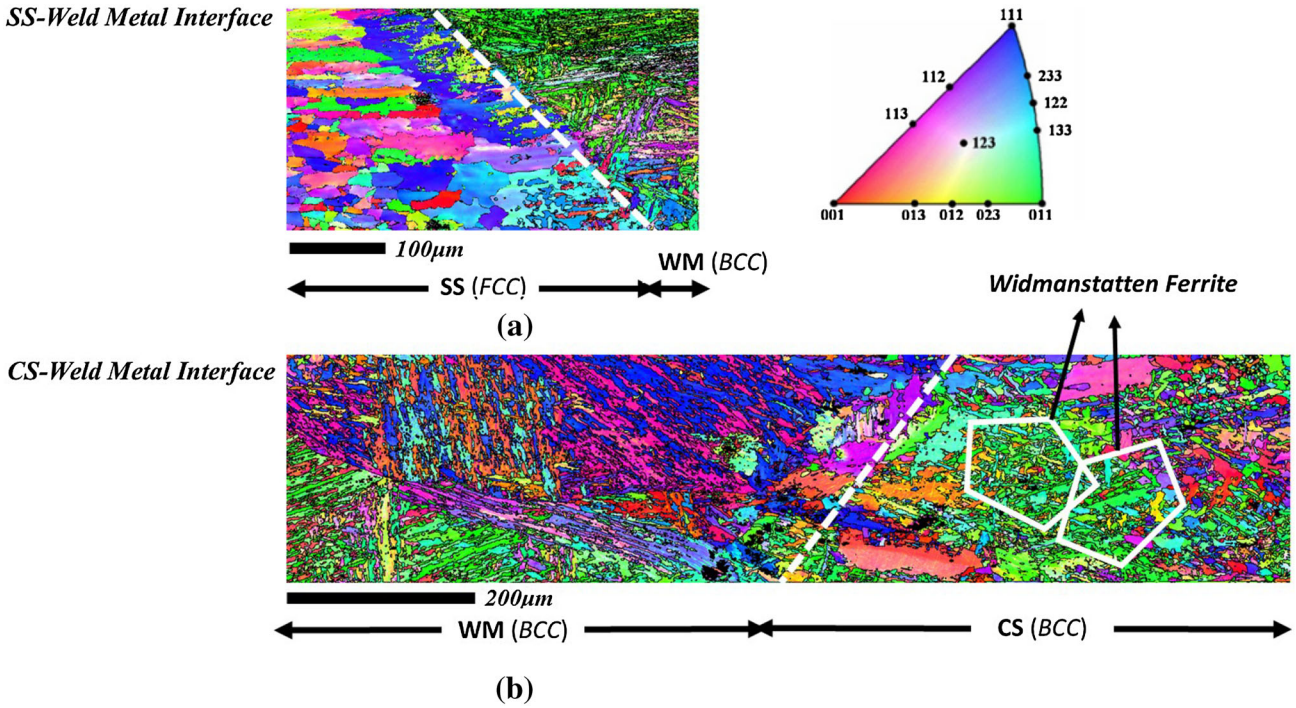

Fig. 4 Inverse pole figure (IPF) map of the **a** SS and weld metal and **b** weld metal and CS of the Z8 weld specimen

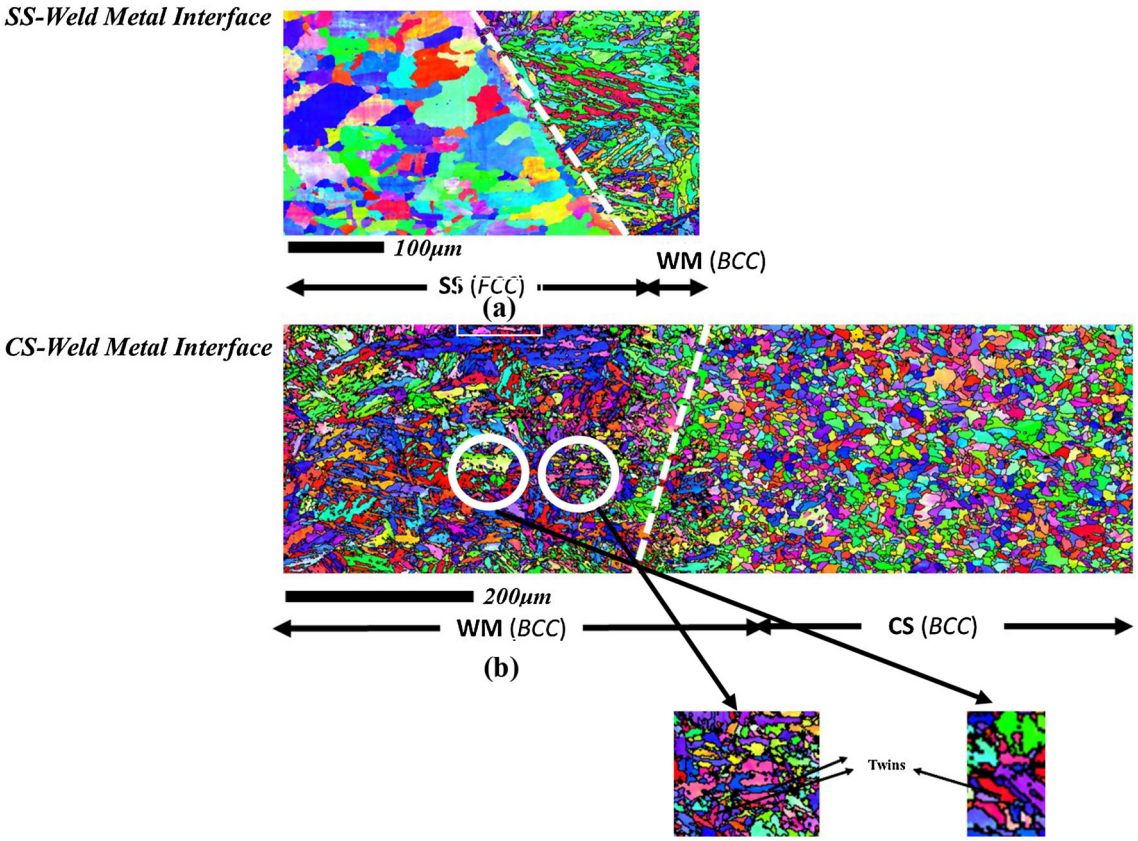

Fig. 5 Inverse pole figure (IPF) map of the **a** SS and weld metal and **b** weld metal and CS of the N9 weld specimen

at different regions of the weld specimen. This is recorded as differences in grain misorientation, grain size and high angle grain boundary (HAGB) fractions as illustrated in Fig. 6.

Microstructure in inverse pole figure (IPF) and phase maps shown in Fig. 7a bring out differences in the phase boundary interface between the SS and weld metal at the fusion zone. The interface in Z8 has an interlock structure while N9 shows a sharp and clear interface.

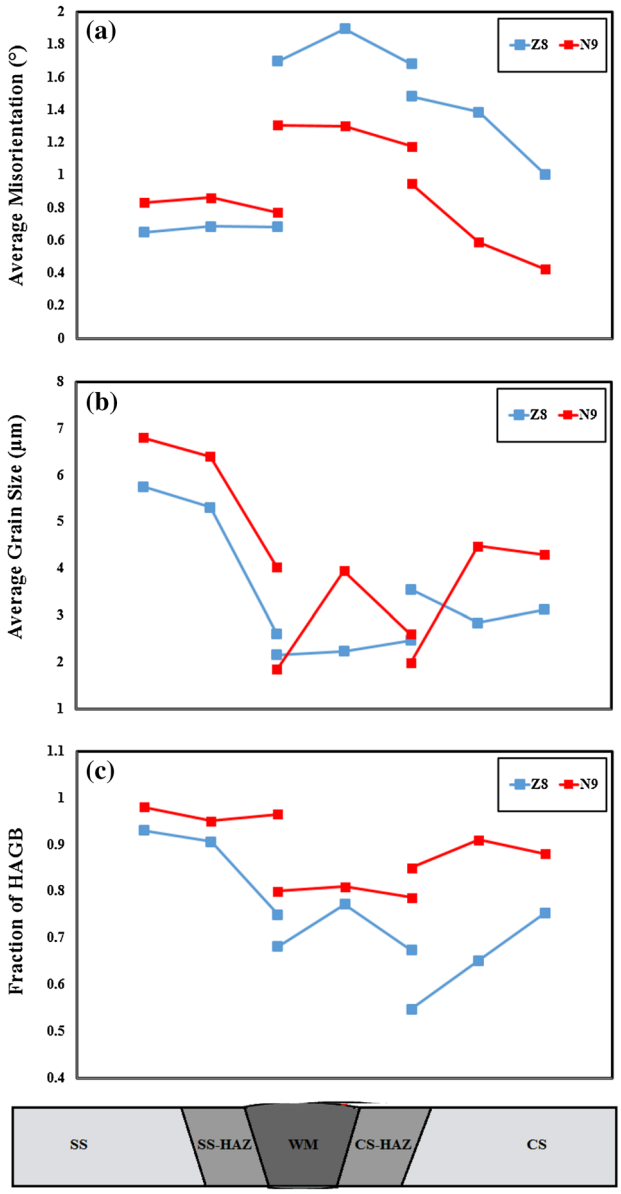

Fig. 6 Clear differences in microstructure parameters estimated through EBSD were observed between Z8 and N9 at different regions of the specimens; **a** average misorientation **b** grain size and **c** fraction of high angle boundaries (HAGB)

3.1 Microstructural Interpretation of the Observed Mechanical Properties

A relationship between the observed mechanical properties and the microstructure development in Z8 and N9 has been presented under this discussion. It was reported in a previous work that the strength of the weld sample was imparted by the HAZ between weld metal and base metal [19]. The tensile strength in the present study was seen higher for Z8 which could be related to higher average in-grain misorienation in the weld metal zone, as observed in Fig. 6a. Recrystallisation was more pronounced in sample N9 at the WM zone, CS-HAZ and SS-HAZ. This was indicated by decreased in-grain misorientation and increased HAGB in the respective zones. In addition Widmanstatten ferrite structure introduced grain refinement in the CS-HAZ of Z8. This improvement in strength might be attributed to the overall grain refinement of the Widmanstatten ferrite. Another important microstructural aspect brought in the present study to explain the lower strength in N9 was the increased fraction of twins in the weld metal region of N9 which could have resulted from recrystallization during annealing. It could be speculated that, following plastic deformation, these twins might have rotated the parent matrix into favorable orientations for slip, enabling easy deformation under the stress fields. These rotations at the onset of plastic deformation by slip could cause the twinned regions to accommodate dislocations and store higher amount of deformation energy with successive deformation.

A clear distinction between the phase interface of SS (FCC crystal structure) and WM (BCC crystal structure) has been brought out for sample Z-8 and N-9 in Fig. 7a. A relatively sharp interface was presented in sample N-9. Further to that, an approximate orientation relationship (OR) of 45° <114> was observed between SS and WM. Such an OR characterizes a phase boundary. The number fraction 45° <114> was highest in Z-8. This was estimtaed manually from 25 to 30 random interfaces of SS and WM in both Z8 and N9. Figure 7b illustrated the number fraction of 45° <114> as a function of the deviation from the exact OR. Also the increased number fraction of OR of 45° <114> in Z8 could hinder the continuity of slip systems of both phases. Dislocation movement was therefore impeded because of mismatch in the slip system. That is why Z8 showed a higer yield strength.

There have been few studies that reported the relationship of hardness with residual stress. However there were differences in the explanations, depending on the materials and the stress states considered [20]. It was usually expected that the maxima in hardness should correspond to the minima of compressive residual stress, however the observed hardness profile in the present weld samples did

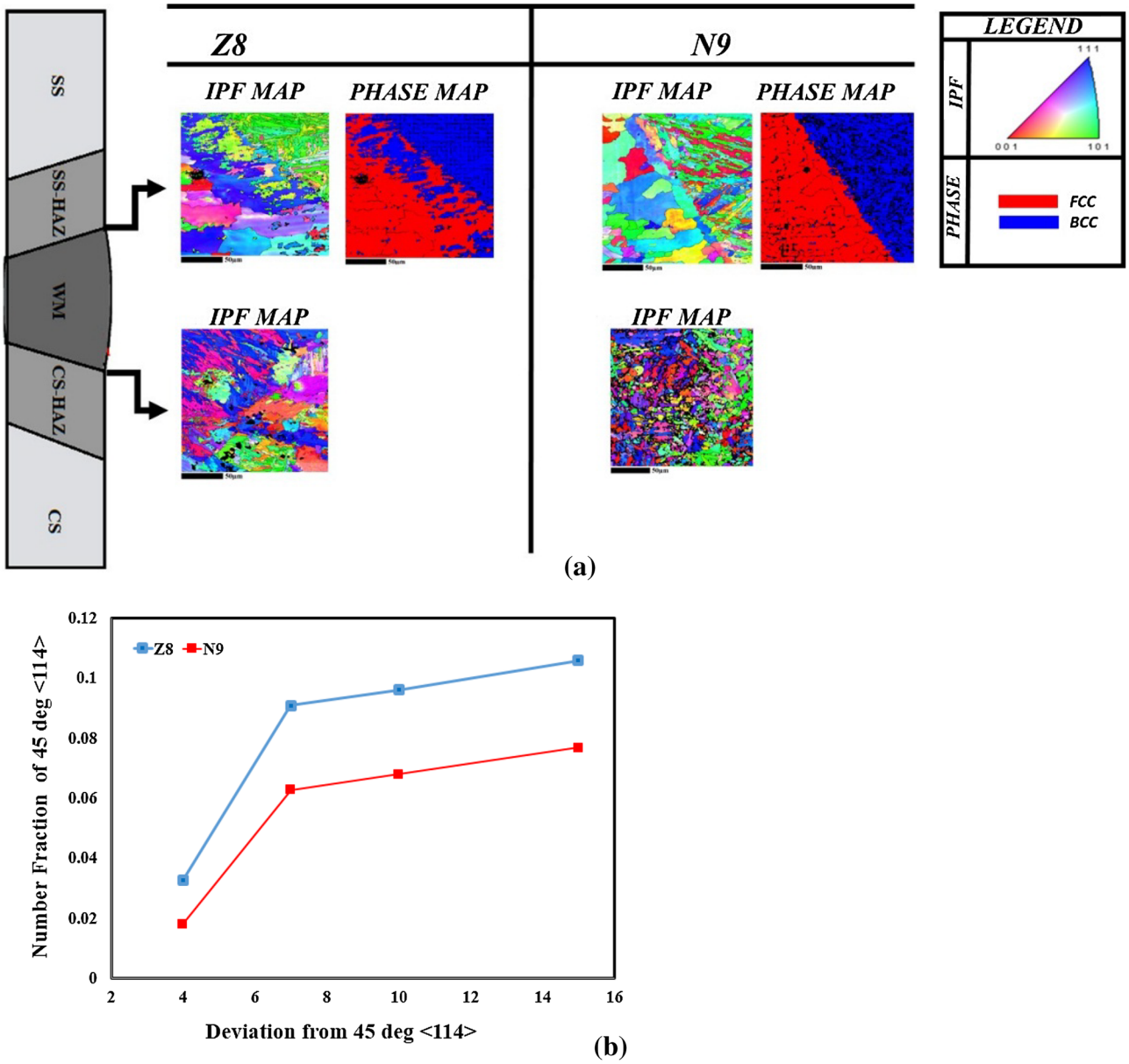

Fig. 7 **a** IPF and phase maps showing the SS and weld metal interface for Z8 and N9. Z8 exhibits an interlocked structure of the two phases; SS (FCC) and weld metal (BCC). **b** Number fractions of 45° <114> phase boundaries as a function of deviation from the exact phase boundary relationship

not show a direct correlation with the residual stress. The measured residual stress along the weld sample surface showed the typical "well-like" profile slightly shifted to the SS side (Fig. 8). This displacement from the center of the weld could be attributed to the differences in thermal expansion between weld metal which had a BCC structure and SS, FCC structure. The heat input during both welding processes spread throughout a broad region. The strongest temperature gradients were expected at the fusion zones and not at the center of the weld metal. Therefore, the fusion zones were the regions that cooled down last. Hence, the stress distribution after completion of welding could arise due to superposition of two peak profiles with each maximum tensile stress appearing asymmetrically or displaced significantly from the weld centerline. The sample Z8 as such exhibited lower compressive (higher tensile) strength than N9. Though no plausible explanation was available to comprehend the variations of stresses for the two samples, but this would be of interest to the authors for their future research work.

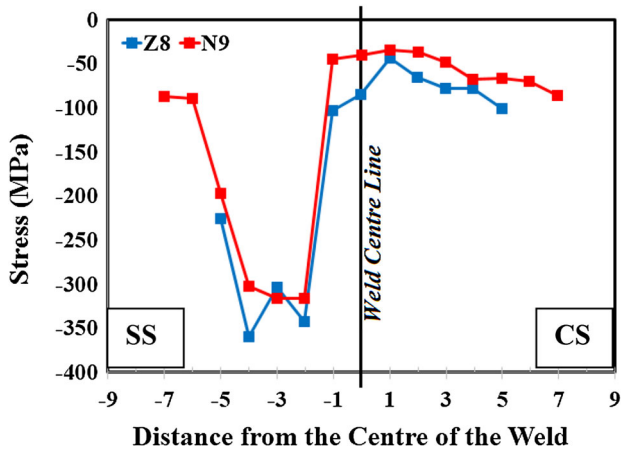

Fig. 8 Compressive residual stresses plotted as a function of the distances from the center of the weld

4 Conclusions

The present study examined the relationship between microstructure investigated through EBSD and mechanical properties in TIG and A-TIG welded specimens. Following conclusions were gathered after systematic microstructural analysis.

- The higher tensile strength of Z8 was mainly attributed to higher in-grain misorientation in the weld metal zone and secondly refinement of grain size in the HAZ of the CS due to formation of Widmanstatten structure.
- The increased number fraction of 45° <114> phase boundaries in sample Z8 additionally imposed hindrance to the continuity of slip system causing dislocations to get locked at these boundaries during deformation leading to higher yield strength.
- No clear correlation between hardness and residual stress was identified. However sample Z8 showed lower compressive residual stress.

Acknowledgments Authors are grateful to Pandit Deendayal Petroleum University (PDPU), Gandhinagar, India and University of Saskatchewan (UoS), Canada for conducting experimental work and high end characterization of the welded samples respectively. Dr Badheka of PDPU is also thankful to the Board for Research in Fusion Science and Technology (BRFST), Institute for Plasma Research (IPR), Gandhinagar, India for sponsoring the research project via project number NFP-08/MAT/01.

References

1. Nayee S G, and Badheka V J, *J Manuf Proc* **16** (2014) 137.
2. Badheka V J, *Weld Cut* **14** (2015) 54.
3. Huang H Y, Shyu S W, Tseng K H, and Chou C P, *J Mater Eng Perform* **17** (2007) 193.
4. Q.M. Li Qing, X.H. Wang, Z. Zou, and J. Wu, *Nonferrous Met Soc China* **486** (2007).
5. Kuo C H, Tseng K H and Chou C P, *Eng Mater* **479** (2011) 74.
6. Radhakrishnan V M, *Welding Technology & Design*, New Age International Publisher, Second edition 2005, ISBN 81-224-1672-1, pp 103.
7. Dhandha K H, Badheka V J, *J Manuf Proc* **17** (2015) 48.
8. Colegrove P, Ikeagu P, Thistlethwaite A, Williams A, Nagy A, Suder W, Steuwer A, and Pirling T, *Sci Technol Weld Join* **14** (2009) 717.
9. Schwartz A J, Kumar M, Adams B L, and Field D, *Electron Backscatter Diffraction in Materials Science*, New York: Springer, (2009).
10. Fujii H, Ueji R, Takada Y, Kitahara H, Tsuji K, Nakata N, and Nogi K, *Mater Trans* **47** (2006) 239.
11. Coelho R S, Kostka A, Pinto H, Riekehr S, Koçak M, and Pyzalla A R, *Mater Sci Forum* **571–572** (2008) 361.
12. Merson E, Hammond C, and Brydson R, Characterization of texture in Ti-6246 alloy fiber laser welds using electron backscattered diffraction, *J Phys Conf Ser* **26** (2006) 347.
13. Kamaya M, Wilkinson A J, and Titchmarsh J M *Nucl Eng Des* **235** (2005) 713.
14. Verlinden B, Driver J, Samajdar I S, and Doherty R D, *Thermo-Mechanical Processing of Metallic Materials*, ISBN-978-0-08-044497-0, Pergamon Materials Series. Series ed. R.W Cahn, Amsterdam:Elsevier, (2007).
15. Taljat B, Radhakrishnan B, and Zacharia T, *Mater Sci Eng A* **246** (1998) 45.
16. Elmer J W, Wong J, and Ressler T, *Mater Trans A* **32** (2001) 1175.
17. Arivazhagan B, and Vasudevan M, *J Manuf Proc* **16** (2014) 305.
18. Tseng K H, *Powder Tech* **233** (2013) 72.
19. Miller D K, Use Undermatching Weld Metal Where Advantageous, Technical Article, Welding Innovation Vol. XIV, No. 1, (1997).
20. Frankel J, Abbate A, and Scholz W, *Expt Mech* 33 (1993) 164.